ELSEVIER

Journal of Nuclear Materials 307–311 (2002) 1507–1512

journal of nuclear materials

www.elsevier.com/locate/jnucmat

Formation and migration of helium bubbles in Fe and Fe–9Cr ferritic alloy

K. Ono [a,*], K. Arakawa [a], K. Hojou [b]

[a] *Department of Material Science, Shimane University, 1060 Nishi-kawatsu, Matsue 690-8504, Japan*
[b] *Japan Atomic Energy Research Institute, Tokai, Ibaraki 319-1195, Japan*

Abstract

Formation and migration of helium bubbles in high purity Fe and an Fe–9Cr ferritic alloy have been studied by in situ electron microscopy and scanning transmission electron microscope–electron energy loss spectrometry (STEM–EELS) analysis. The swelling under irradiation with 10 keV He^+ ions in the ferritic alloy was retarded in the low fluence region at 400 °C and was reduced at 600 °C even under heavy irradiation. These results suggest trapping effects of vacancies by Cr and its modulation with helium atoms in the bubble formation. Furthermore, it is found that the mean square of the bubble migration distance in both materials is proportional to time, which is a quantitative evidence of Brownian type motion and yields lower diffusivities of the bubbles in Fe–9Cr than in Fe. The retardation of the bubble mobility in Fe–9Cr should be caused by Cr segregation on the bubble surface which was revealed by STEM–EELS analysis.

1. Introduction

High (9–12 wt%) Cr base steels are recognized as a leading candidate for first wall structure materials [1], and a number of work has been reported and reviewed [2,3]. Great swelling resistance in ferritic/martensitic steels may reside primarily in delay of voids nucleation, but is complexly dependent on temperature, composition (crystal structure), dpa-rate and also helium generation rate. To accept a general understanding on the swelling resistance mechanism, more fundamental experiments are required.

The formation and migration of gas bubbles are fundamental processes of the void swelling and their in situ information is greatly worthy for the study of swelling resistance mechanisms. However, little information on Cr affected bubble behavior, in particular dynamical bubble behavior, is available even in simple ferritic Fe–Cr binary alloy. Therefore, in the present work, we aimed to examine Cr effects on the formation and migration of bubbles, by comparing Fe with Fe–9Cr which was irradiated with such low-energy helium ions as in a fusion plasma and utilizing in situ observation technique which has been successfully established [4,5].

2. Experimental procedures

Specimens were 99.999 at.% Fe supplied by Showa Denko Co. and an Fe–9wt%Cr ferritic alloy, which was cast from high purity starting materials supplied by Johnson–Matthey. Disk shaped specimens of these materials were pre-annealed at 1070 °C for 1 h in an ultra-high vacuum furnace and then electrochemically polished for transmission electron microscopy (TEM). The specimen was mounted on a TEM specimen holder, Gatan-652, for high temperatures and irradiated with 10 keV He^+ ions, using a low energy ion accelerator connected to a JEOL-2010 electron microscope. In situ TEM observation of the damage evolution in the specimen was performed during ion irradiation with a constant flux of 5.0×10^{17} ions/m^2 s (peak dpa-rate $\simeq 5 \times 10^{-4}$ s^{-1} [6]) at temperatures from 200 to 800 °C. Some specimens irradiated with He^+ ions were

* Corresponding author.
E-mail address: onokotar@riko.shimane-u.ac.jp (K. Ono).

0022-3115/02/$ - see front matter
PII: S0022-3115(02)01268-0

annealed stepwise from 400 to 1000 °C and the motion of the bubbles was continuously monitored, using a video recording system with a CCD camera. The path of a bubble was followed by using an image processor, which allows systematic measurements of the center position of the bubbles as a function of time.

To examine the precipitation or segregation of Cr in irradiated or un-irradiated specimens, STEM–EELS analysis was performed, using a type JEOL-2000F TEM with a field emission gun, and Gatan-766 (Digi-PEELS). Scanning of the electron probe with the diameter 1 nm was made by 0.12 nm space and EELS spectra from L_{23} edges of Fe and Cr were measured.

3. Results and discussion

3.1. Formation of interstitial loops

Interstitial type dislocation loops were formed in pure Fe and Fe–9Cr at 200 and 400 °C, but rarely formed at 600 °C. The areal number densities of the loops in these materials were in the range from 1.5×10^{15} to 8×10^{15} m^{-2} at 200 °C and from 2×10^{15} to 5×10^{15} m^{-2} at 400 °C, increasing with the fluence from 2×10^{18} to 5×10^{19} ions/m^2, where the densities in Fe–9Cr were about 50% higher than that in pure Fe. However, the total length of the loop dislocations, calculated by sum up of the loop circles, was just the same in both materials. This fact suggests that dislocation sink effects for bubble formation are the same in both materials under the present experimental conditions, although sink bias effects of dislocation loops for void swelling were frequently quoted in the case of neutron irradiation [7–9]. The enhanced nucleation mechanism of the dislocation loops in pure Fe under the irradiation with helium ions has been discussed elsewhere [10].

3.2. Formation of helium bubbles

At 200 °C, a high density of bubbles were formed around the projected ion range of 20–70 nm [6]. Their number density saturated at around 1.7×10^{17} m^{-2} in both materials under irradiation from 1×10^{20} to 2×10^{21} ions/m^2. The Corresponding diameter of the bubbles increased from 1.1 to 2.2 nm in Fe, while the increase in Fe–9Cr was limited from 1.1 to 1.5 nm. This indicates that the growth rate of the bubble in Fe was significantly faster than that in Fe–9Cr.

The size distributions of bubbles formed at 400 and 600 °C are shown in Fig. 1. The shape of these bubbles was almost spherical at 400 °C, but frequently faceted at 600 °C. As seen in the figure, the areal number density of bubbles in Fe–9Cr at 400 °C was in the order of 10^{16} m^{-2} and almost the same with that in Fe, if the fluence was lower than 3×10^{20} ions/m^2. However, at higher fluence, the density was higher than that in Fe where the growth and coalescence (without motion) of bubbles were sig-

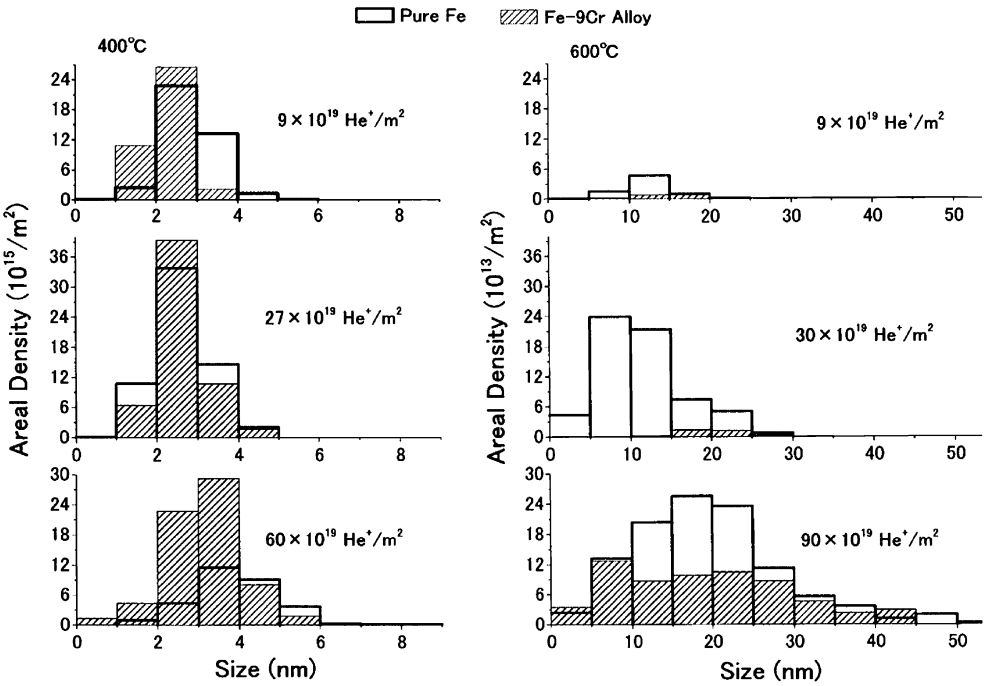

Fig. 1. Size distribution of bubbles in Fe and Fe–9Cr which were irradiated to each fluence at 400 and 600 °C, respectively.

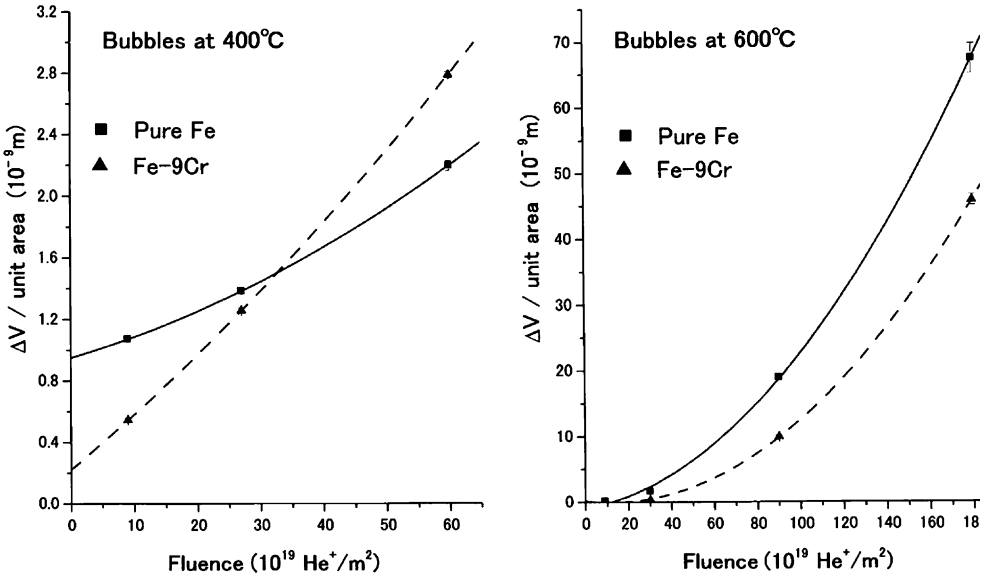

Fig. 2. Total volume of bubbles per unit area in Fe and Fe–9Cr which were irradiated at 400 and 600 °C, respectively, versus the fluence.

nificant. At 600 °C, the bubble densities in both materials drastically decreased to the order of 10^{14} m^{-2}, but the density in Fe–9Cr was lower than in Fe even by irradiation to higher fluence. Bimodal cavity distribution [11] was not observed in the present work.

The total volume of these bubbles per unit area, ΔV, is shown in Fig. 2. It is clearly known that Cr suppresses the swelling in the low fluence region ($<3.5 \times 10^{20}$ ions/m^2) at 400 °C, where the concentration of Cr is higher than that of He in the irradiated region [6]. However, the swelling manner is reversed at higher fluence. These results suggest that the appearance of visible bubbles in Fe–9Cr is retarded by Cr, interacting with vacancies which lead to the bubble nucleation and growth. The invisible bubbles grow up with the increase of irradiation, where the concentration of He is higher than of Cr and then the direct interaction process between vacancy and He becomes dominant. Although a similar Cr affected incubation was pointed out in neutron-irradiated ferritic alloys [12], those relative effects between Cr and He concentrations were found out in the present work.

At 600 °C, the swelling reverse manner as observed at 400 °C did not appear as seen in Fig. 2, which suggests a minor role of incubation effects by Cr as pointed out at 400 °C. Beside, the drastic decrease of area bubble densities, as shown in Fig. 1, suggests a remarkable break-up of bubble embryos at 600 °C and that the break-up is particularly significant in Fe-9Cr. Therefore, these results suggest an operation of a different mechanism in the nucleation process of bubbles at 600 °C. One possible mechanism is that a comparatively strong interaction between vacancy and helium [13] should be weakened by addition of large atomic size Cr [14] and then surviving of bubble embryos becomes difficult in the alloy. However, well nucleating bubbles should be stabilized and retarded in their mobility by Cr segregated on the bubble as shown in the following section.

3.3. Annealing and bubble motion

After He^+ ion irradiation at 400 °C to the fluence of $3–9 \times 10^{19}$ ions/m^2, the specimen was isochronally annealed for 20 min at higher temperatures and changes in size and density of bubbles were examined. It was found that smaller bubbles (diameter $r \approx 1$ nm) disappeared and larger bubbles ($r \approx 4–6$ nm) appeared above 650 °C in Fe, while, in Fe–9Cr, a similar size change appeared above 700 –750 °C. These size changes were caused by bubble migration and coalescence. Therefore, these facts indicate that the mobility of bubbles in Fe–9Cr is much lower than that in Fe.

To quantify the helium bubble mobility, the video image of moving bubbles was analyzed. Fig. 3 shows a sequence of video frames taken at 750 °C on the Fe specimen, following the irradiation to a fluence of 6×10^{19} ions/m^2 at 300 °C and warming up stepwise. The random motion, depending on the bubble size, and coalescence of bubbles are clearly seen. The path of the moving bubbles was measured for several annealing temperatures at time intervals of 2 s. Details of the image processing has been reported elsewhere [4,5]. In Fig. 4, an example of the mean square of the migration distance, $\langle R^2 \rangle$, for bubbles of several size in Fe–9Cr is

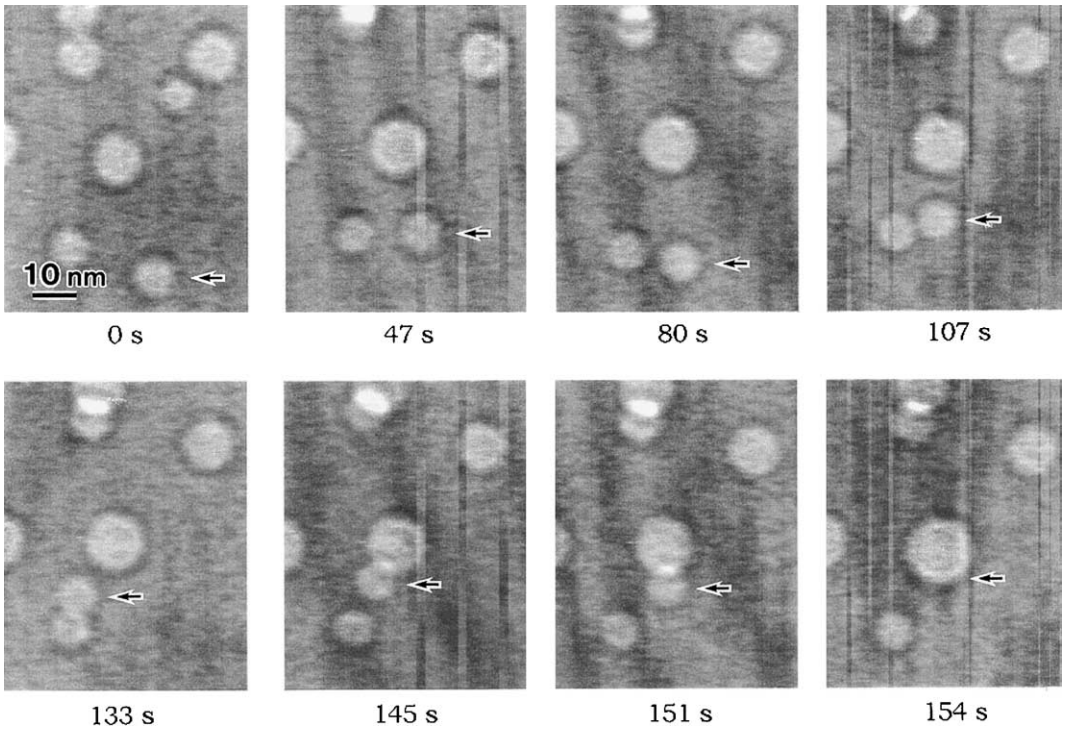

Fig. 3. A sequence of video frames which shows a profile of bubble motion at 750 °C in Fe.

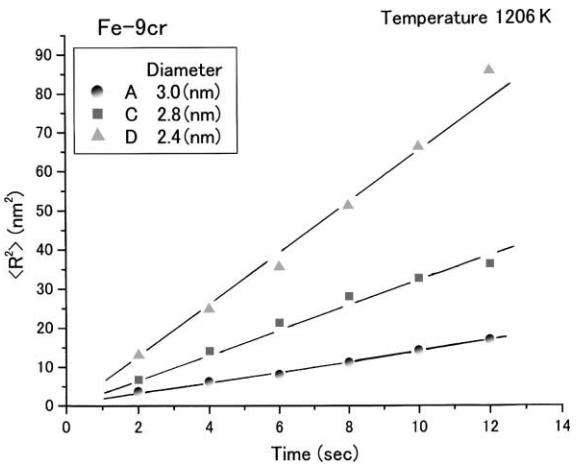

Fig. 4. Mean squares of the migration distance of bubbles with 2.4–3.2 nm diameter in Fe–9Cr at 933 °C as a function of time.

plotted as a function of time t. It is evident that $\langle R^2 \rangle$ is proportional to time t for each bubble. This is a quantitative evidence of Brownian type motion of bubbles and is the first demonstration in the ferritic alloy.

According to the random walk theory, we can successfully estimate the diffusion coefficient of bubbles, D, from a relation $D = \langle R^2 \rangle / 4t$, if the proportional relation

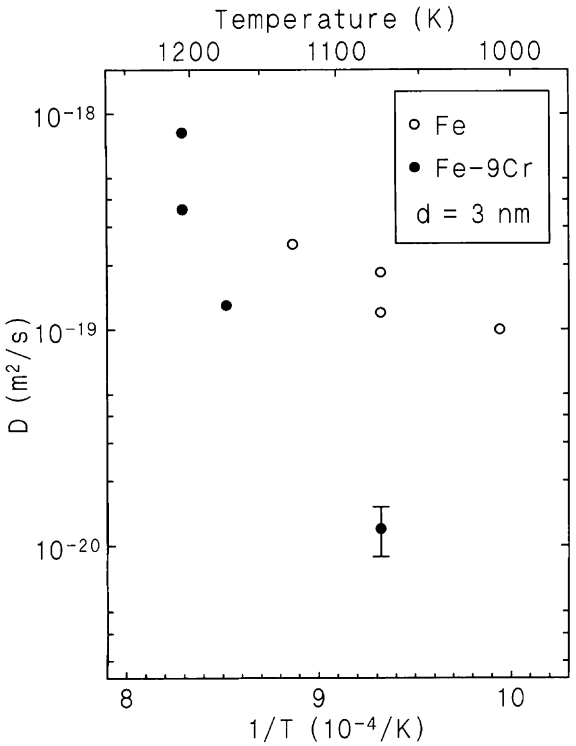

Fig. 5. Diffusivity of bubbles with about 3 nm diameter in Fe and Fe–9Cr versus $1/T$.

between D and t is well established as shown in Fig. 4. Thus the obtained diffusion coefficients of bubbles with about 3 nm diameter in Fe and Fe–9Cr are compared in Fig. 5. These data are a little scattered from Arrhenius relation because of a slight difference in the bubble size, but it is evident that the diffusivity of the bubble in Fe–9Cr is much lower than that in Fe at temperatures lower than about 900 °C.

3.4. Cr segregation or precipitation in the alloy

A Chromium rich phase or Cr precipitates were frequently induced in the Fe–9Cr matrix, grain boundary and specimen surface by irradiation above 400 °C. STEM–EELS analysis results on the bubble surface, measured at room temperature are shown in Fig. 6, where the upper half is an annular dark field (ADF) image of the bubble in the Fe–9Cr specimen irradiated to 2×10^{20} He^+/m^2 at 600 °C and annealed at 850 °C for 10 min, and the lower half indicates distributions of Fe and Cr which were obtained by measuring EELS spectra from L_{23} edges along the white line in the ADF image. The number of electrons in the vertical axis was calculated by subtracting the background intensity from each edge of raw spectra. As seen from the figure, the decrease of Fe due ot the bubbles and the increase of Cr around the bubbles are evident. There were no heterogeneous matrix effects such as precipitate clusters around the bubble, which may influence the line scanning. Although the STEM–EELS measurement was tried at high temperatures, the drifting of the ferritic alloy sample during the electron probe scanning was not negligible and the element mapping at high temperature was unsuccessful. However, the specimen shown in Fig. 6 was quickly cooled down to room temperature. Therefore, we consider, the segregation manner of Cr on the bubble surface should be same with that at high temperatures around 850 °C.

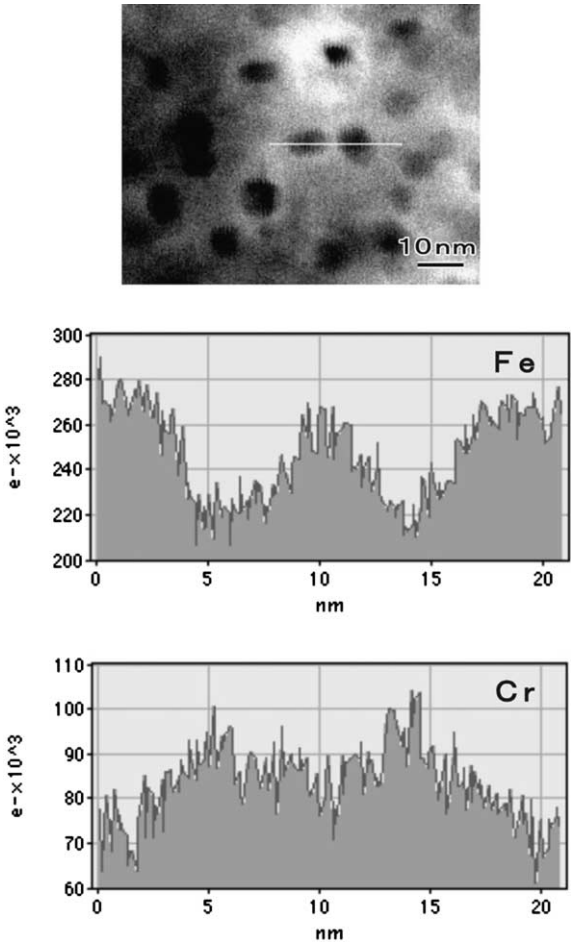

Fig. 6. ADF image of the bubbles in an Fe–9Cr specimen, and Fe and Cr distributions which were measured by STEM–EELS along the white line in the ADF image.

The difference between bubble diffusivities in Fe and Fe–9Cr is evident from the present laborious work, as shown in Fig. 5. Therefore, we can conclude that the Cr segregation on the bubble surface, which should cause retardation of the bubble surface diffusion, should be one of important reasons of the retarded bubble motion.

4. Conclusions

We have examined the formation and migration of helium bubbles in Fe and an Fe–9Cr ferritic alloy by in situ TEM with 10 keV He^+ ions irradiation and STEM–EELS analysis and concluded as follows:

1. The sink density of the interstitial type dislocation loops for the bubble formation was the same in both materials at 200–400 °C.
2. The swelling in Fe–9Cr was retarded in low fluence regions at 400 °C and was reduced even in heavy irradiation at 600 °C. These results suggested trapping effects of vacancies by Cr and weakening effects of the interaction between helium atoms and vacancies by adding Cr.
3. The mean square of the bubble migration distance was proportional to time in both materials, which is a quantitative evidence of Brownian type motion and yielded lower diffusivity in Fe–9Cr than in pure Fe.
4. STEM–EELS analysis revealed segregation of Cr on the bubble surface, which causes the retardation of the bubble motion.

References

[1] A. Kohyama, A. Hishinuma, D.S. Gell, R.L. Klueh, W. Dietz, K. Ehrlich, J. Nucl. Mater. 233–237 (1996) 138.
[2] D.L. Klueh, D.L. Harries, High-Chromium Ferritic and Martensitic Steels for Nuclear Applications, ASTM Stock Number: MONO3, 2001.
[3] F.A. Garner, M.B. Toloczko, B.H. Sencer, J. Nucl. Mater. 276 (2000) 123.
[4] K. Ono, K. Arakawa, M. Oohashi, H. Kurata, K. Hojou, N. Yoshida, J. Nucl. Mater. 283–287 (2000) 210.
[5] K. Ono, K. Arakawa, K. Hojou, M. Oohashi, R.C. Birtcher, S.E. Donnelly, J. Electron Microsc. 51 (2002) S245.
[6] J.P. Biersack, L.G. Haggmark, Nucl. Instrum. and Meth. 174 (1986) 257.
[7] E.A. Little, R. Bullough, M.H. Wood, Proc. Roy. Soc. Lond. A 372 (1980) 565.
[8] D.S. Gelles, J. Nucl. Mater. 108&109 (1982) 515, 225 (1995) 163.
[9] Y. Katoh, A. Kohyama, D.S. Gelles, J. Nucl. Mater. 225 (1995) 154.
[10] K. Arakawa, R. Imamura, K. Ohta, K. Ono, J. Appl. Phys. 89 (2001) 4752.
[11] L.L. Horton, L.K. Mansur, ASTM STP 870 (1985) 344.
[12] E.A. Little, D.A. Stow, J. Nucl. Mater. 87 (1979) 25.
[13] W.D. Wilson, Radiat. Eff. 78 (1983) 11.
[14] H.W. King, J. Mater. Sci. 1 (1966) 79.